Mon. Not. R. Astron. Soc. **394,** L11–L15 (2009) doi:10.1111/j.1745-3933.2008.00597.x

The effect of gas physics on the halo mass function

R. Stanek,[1⋆] D. Rudd[2] and A. E. Evrard[1,3]

[1]*Department of Astronomy, University of Michigan, 500 Church St, Ann Arbor, MI 48109, USA*
[2]*School of Natural Sciences, Institute for Advanced Study, Einstein Drive, Princeton, NJ 08540, USA*
[3]*Department of Physics and Michigan Center for Theoretical Physics, University of Michigan, 450 Church St, Ann Arbor, MI 48109, USA*

Accepted 2008 November 10. Received 2008 October 29; in original form 2008 September 16

ABSTRACT

Cosmological tests based on cluster counts require accurate calibration of the space density of massive haloes, but most calibrations to date have ignored complex gas physics associated with halo baryons. We explore the sensitivity of the halo mass function to baryon physics using two pairs of gas-dynamic simulations that are likely to bracket the true behaviour. Each pair consists of a baseline model involving only gravity and shock heating, and a refined physics model aimed at reproducing the observed scaling of the hot, intracluster gas phase. One pair consists of billion-particle resimulations of the original $500\,h^{-1}$ Mpc Millennium Simulation of Springel et al., run with the smoothed particle hydrodynamics (SPH) code GADGET-2 and using a refined physics treatment approximated by pre-heating (PH) at high redshift. The other pair are high-resolution simulations from the adaptive-mesh refinement code ART, for which the refined treatment includes cooling, star formation and supernova feedback (CSF). We find that, although the mass functions of the gravity-only (GO) treatments are consistent with the recent calibration of Tinker et al. (2008), both pairs of simulations with refined baryon physics show significant deviations. Relative to the GO case, the masses of $\sim 10^{14}\,h^{-1}\,\mathrm{M}_{\odot}$ haloes in the PH and CSF treatments are shifted by the averages of -15 ± 1 and $+16 \pm 2$ per cent, respectively. These mass shifts cause $\sim$30 per cent deviations in number density relative to the Tinker function, significantly larger than the 5 per cent statistical uncertainty of that calibration.

Key words: galaxies: clusters: general – cosmology: theory.

1 INTRODUCTION

Deep cluster surveys offer the promise of tightly constraining cosmological parameters, including the nature of dark energy (Holder, Haiman & Mohr 2001; Levine, Schulz & White 2002; Majumdar & Mohr 2003; Lima & Hu 2004, 2005; Younger et al. 2006; Sahlén et al. 2008). Realizing this promise requires accurate calibration of the expected counts and clustering of massive haloes, along with a careful treatment of how halo mass relates to the signals observed by such surveys. This logical division is reflected by two long-standing threads of effort, one focused on the emergence of massive structures from gravity and the other focused on scaling relations of multiple signals within the population of massive haloes.

The fact that 17 per cent of clustered matter in the universe is baryonic ties these threads together. Non-gravitational physics is required in massive haloes, not simply to create galaxies (White & Rees 1978) but also to reproduce scaling behaviour of the hot, intracluster medium (ICM) observed in X-rays (Evrard & Henry 1991; Borgani et al. 2001; Reiprich & Böhringer 2002; Stanek et al. 2006; Nagai, Vikhlinin & Kravtsov 2007). If a significant fraction of halo baryons becomes spatially segregated from the dark matter either condensed within galaxies or disbursed from non-gravitational heating, then the gravitational development of massive structures will be altered, perhaps at the $\sim$10 per cent level, under strong baryonic effects.

The spatial number density of haloes or mass function expected from Gaussian random initial conditions was originally derived using a mix of analytic arguments and numerical simulations (e.g. Press & Schechter 1974; Bond et al. 1991; Sheth & Tormen 1999). Modern efforts focus on providing fitting functions of increasing statistical precision (Jenkins et al. 2001; Warren et al. 2006; Tinker et al. 2008). The recent Tinker et al. (2008) mass function (hereafter TMF), calibrated to a wide range of cosmological simulations that include gas-dynamic, Marenostrum simulations (Gottlöber & Yepes 2007; Yepes et al. 2007), has pushed statistical errors to the level of 5 per cent.

To date, however, there have been a few gas-dynamic simulations that include a non-gravitational treatment of baryonic processes in volumes large enough to provide good statistics for high-mass haloes. Calibration of the mass function at the level of the Tinker et al. (2008) using hydrodynamic simulations is too expensive to be feasible in the near term. A less computationally expensive technique is to compare realizations of fixed initial conditions evolved

⋆E-mail: rstanek@umich.edu

with different baryonic physics. Jing et al. (2006) and Rudd, Zentner & Kravtsov (2008) employ this approach to study baryonic effects on the matter power spectrum, finding 2–10 per cent modifications of the matter power spectrum at scales $k \sim 1\ h\,\mathrm{Mpc}^{-1}$. Rudd et al. (2008) finds a halo mass function that is enhanced by ∼10 per cent relative to the dark matter only case. Neither set of simulations was sufficiently large to properly probe rich cluster scales, however.

In this letter, we take a similar approach to examine the effect of non-gravitational, baryonic physics on the cluster mass function. Specifically, we consider two pairs of gas-dynamic simulations, each comprised of a treatment of the gas with gravity and shock heating only and a second, more complicated treatment. One pair are Millennium Gas Simulations (MGS Hartley et al. 2008), with smoothed particle hydrodynamics (SPH) gas dynamics under GADGET-2 (Springel 2005), and the second pair are adaptive-mesh ART simulations from Rudd (2007). As the two simulations in each pair have the same initial conditions, we infer the effects of baryonic physics by comparing haloes in the more detailed simulations with their gravity-only (GO) counterparts. The outline of this paper is as follows. In Section 2, we discuss the various simulations and their bulk cluster properties, comparing them to observations. Section 3 compares halo masses between corresponding haloes in each pair of simulations, and discusses the effect on the total mass function. All haloes masses are identified as M_{500}, the mass of a spherical halo with radius r_{500} and mean density $500\rho_c(z)$, where $\rho_c(z)$ is the critical density of the universe.

2 SIMULATIONS AND HALO SAMPLES

We use two pairs of gas dynamic simulations, each pair run from a single set of initial conditions and differing only in the included physical processes. Our baseline simulations are evolved with GO, shock heating and adiabatic processes acting on the gas and a second has more complicated treatment of the gas physics discussed below.

Haloes in all simulations are identified as spherical regions, centred on the peak of the dark matter distribution, where the mean enclosed density is 500 $\rho_c(z)$. Our analysis focuses on $z = 0$ and 1 samples, redshifts that roughly bracket the range important for dark energy studies. When calculating the bulk cluster properties, we exclude from our sample haloes that overlap with more massive neighbours, however, to remain consistent with Tinker et al. (2008) haloes that overlap but whose centres lie outside their respective virial radii are included in the mass function analysis.

2.1 Millennium gas simulation

The MGS are a pair of resimulations of the Millennium Simulation (Springel et al. 2005), a high-resolution, dark-matter-only simulation of a $500\,h^{-1}$ Mpc cosmological volume. Like the original Millennium Simulation, the simulations were run with GADGET-2, which treats the gas dynamics with the SPH (Springel 2005). The MGS runs use a down-sampled version of the initial conditions of the Millennium Simulation, with 5×10^8 dark matter particles, each of mass $1.4 \times 10^{10}\,h^{-1}\,\mathrm{M}_\odot$, and 5×10^8 SPH gas particles, each of mass $3.1 \times 10^9\,h^{-1}\,\mathrm{M}_\odot$. This mass resolution is about 20 times coarser than the original Millennium Simulation, and the gravitational softening length of $25\,h^{-1}$ kpc is correspondingly larger. The cosmological parameters match the Millennium Simulation: $(\Omega_m, \Omega_b, \Omega_\Lambda, h, n, \sigma_8) = (0.25, 0.045, 0.75, 0.73, 1.0, 0.9)$.

Complementing the aforementioned GO realization is an MGS simulation with cooling and PH, denoted as PH. PH is a simple approximation that assumes high redshift galaxy formation feedback drove the proto-ICM gas to a fixed entropy level, after which the ICM evolves under hierarchical gravity (Evrard & Henry 1991; Kaiser 1991; Bialek, Evrard & Mohr 2001). In our implementation, the entropy of each gas particle is instantaneously boosted to 200 keV cm^2 at $z = 4$. The gas is allowed to radiatively cool thereafter using the cooling function of Sutherland & Dopita (1993), but the cold gas fraction is very small. The entropy level of the PH model is tuned to match bulk X-ray observations of clusters at redshift zero, as we discuss shortly.

For both MGS models, we calculate bulk cluster gas properties with primary haloes of mass $M_{500} \geq 5 \times 10^{13}\,h^{-1}\,\mathrm{M}_\odot$, yielding sample sizes of 2527 (PH) and 3446 (GO) at $z = 0$, and of 475 (PH) and 818 (GO) at $z = 1$. For the mass function analysis, we extend the mass cut to $M_{500} \geq 10^{13}\,h^{-1}\,\mathrm{M}_\odot$.

2.2 ART simulations

Our second set of models are simulated using the distributed-parallel hydrodynamic ART code (Rudd et al. 2008; Rudd 2007). The simulations evolve a $240^3\,h^{-3}\,\mathrm{Mpc}^3$ volume of a *Wilkinson Microwave Anisotropy Probe 3* (*WMAP*3)-motivated cosmological model with parameters $(\Omega_m, \Omega_b, \Omega_\Lambda, h, n, \sigma_8) = (0.25, 0.042, 0.75, 0.73, 0.95, 0.8)$. The baseline GO simulation was performed using 512^3 dark matter particles with mass $m_p \sim 5.9 \times 10^9\,h^{-1}\,\mathrm{M}_\odot$ and allow for four levels of refinement achieving a minimum cell size of $240\,h^{-1}\,\mathrm{Mpc}/(512 \times 2^4) \approx 29\,h^{-1}$ kpc. The ART–GO simulation has 244 haloes over a mass cut of $5 \times 10^{13}\,h^{-1}\,\mathrm{M}_\odot$. We then selected the 13 most massive haloes in the simulation volume at $z = 0$, and resimulated at 1024^3 effective resolution ($m_p \approx 7.4 \times 10^8\,h^{-1}\,\mathrm{M}_\odot$) the regions within 5 $r_{vir} \sim 5$–$10\,h^{-1}$ Mpc surrounding each cluster centre. This simulation includes prescriptions for star formation and metal-dependent radiative cooling described in Rudd (2007). For this simulation, the same 512^3 uniform mesh was used, but in the high-resolution regions seven levels of refinement were used for a peak spatial resolution of $\approx 3.6\,h^{-1}$ kpc.

2.3 Baryon Census

We begin by exploring the bulk properties of baryons in the massive halo samples as a means of assessing the viability of the different physical treatments.

Fig. 1 shows baryon mass fractions within r_{500}, normalized to the universal baryon fraction Ω_b/Ω_m. In the GO simulations, all the baryons are in the hot ICM phase, so that $f_b = f_{ICM}$. In the CSF simulation, gas is removed from the hot phase through radiative cooling and converted to stars. For these haloes, we plot both the ICM mass fraction f_{ICM} and the total baryon fraction, $f_b = f_{ICM} + f_{cond}$, where condensed baryons, f_{cond}, includes both stars and cold gas ($T < 2 \times 10^5$ K). Although the PH model allows radiative cooling, the fraction of cold gas in our halo samples is very small, less than 2 per cent of the baryons.

The GO simulations display constant baryon fractions that are slightly suppressed from the universal mean value. The level of suppression is somewhat larger in the MSG haloes compared to the ART sample, which is consistent with the difference between SPH and grid codes reported by Kravtsov, Nagai & Vikhlinin (2005). The mass-limited samples have average baryon fractions at $z = 0$ of $f_b = 0.89 \pm 0.025$ and 0.93 ± 0.038, respectively. The MGS baryon fractions are consistent with those in SPH simulations done at similar resolution and measured within $\Delta_c = 200$ by Crain et al. (2007) and Ettori et al. (2006).

The baryon distributions in the PH and CSF simulations are more complicated. In the PH case, the entropy increase at

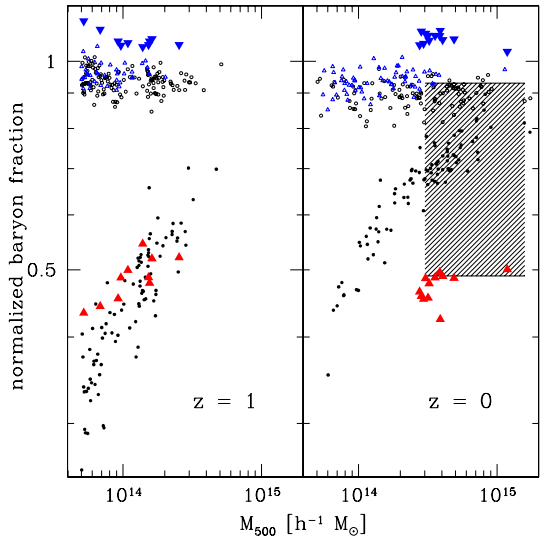

Figure 1. Baryon fractions as a function of total halo mass at $z = 1$ (left-hand panel) and $z = 0$ (right-hand panel) are shown for the MGS halo samples in the GO (open circles) and PH (filled circles) treatments and for the ART samples in the GO (open triangles) and CSF (filled triangles) cases. For this latter, regular triangles show the ICM mass fraction while inverted triangles show the total baryon fraction (gas plus stars) within the haloes. The shaded region shows the 90 per cent confidence range of the mean, observed ICM mass fraction inferred for local, $kT > 4$ keV clusters by Vikhlinin (2006). For clarity, only a subset of the MGS samples is shown for masses below $4 \times 10^{14}\,M_\odot$.

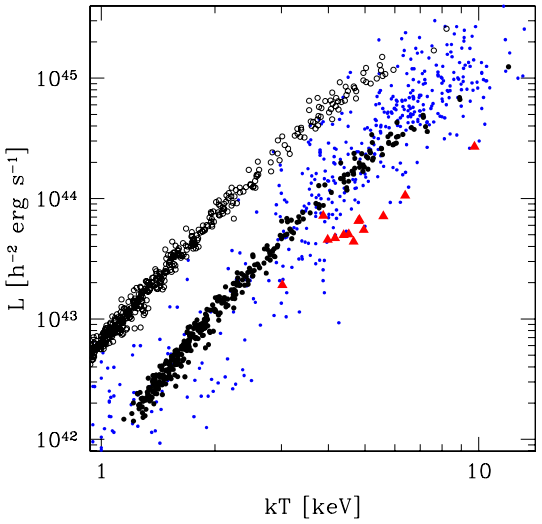

Figure 2. The $L_{\rm bol}$–$T_{\rm sl}$ relations for the MGS–GO (open circles), MGS–PH (filled circles) and ART–CSF (filled triangles) samples are compared to observations (small points) compiled by Hartley et al. (2008). The MGS haloes are subsampled as in Fig. 1.

$z \sim 4$ causes the gas to expand, especially in lower-mass haloes for which the characteristic entropy is lower, and raises the sound speed throughout the proto-ICM. The latter effect pushes the effective shock radius to larger values compared to the purely gravity-driven case (Voit et al. 2003). As a result, lower-mass haloes retain a smaller fraction of their baryons within r_{500}, leading to the mass-dependence seen in Fig. 1. Since the characteristic halo entropy increases with time at fixed mass, the mean ICM gas fraction at fixed mass increases from $z = 1$ to 0 in the PH haloes. At $z = 0$, the highest mass haloes have baryon fractions suppressed by only 10 per cent relative to the GO treatment.

In the CSF haloes, the hot gas fraction, $f_{\rm ICM}$, is comparable to that in the PH clusters of similar mass at $z = 1$. However, the total baryon fraction in these haloes is close to universal due to the contribution of cold gas and stars. Unlike the PH models, the ICM mass fraction does not evolve with time, remaining approximately constant at $\approx$50 per cent from $z = 1$ to 0, even as the clusters themselves grow by a factor of 2 in total mass. The total baryon fraction grows by 4 per cent due primarily to the small increase in the ICM. The stellar component grows significantly from $\sim$40 to $\sim$47 per cent but is balanced by a corresponding decrease in the fraction of cold gas from $\sim$10 to $\sim$4 per cent.

As an empirical test of the models, we show in Fig. 2 the scaling between bolometric luminosity $L_{\rm bol}$ and spectral temperature $T_{\rm sl}$ for the $z = 0$ halo samples of the MGS and ART–CSF simulations. The models are compared to a local sample of clusters compiled by Hartley et al. (2008). As the local sample extends only to modest redshifts, $z \lesssim 0.2$, we do not apply evolutionary corrections to the observations.

For the models, we use the analytic approximation of Bartelmann & Steinmetz (1996) to compute $L_{\rm bol}$ within r_{200} of each halo. For all MGS haloes, we compute spectroscopic temperatures, $T_{\rm sl}$, using the expression in Mazzotta et al. (2004). This expression is insufficient for large quantities of low-temperature gas, so, for the CSF clusters, we use instead the method of Vikhlinin (2006). Additionally, for the CSF clusters, we exclude gas within $0.1r_{200}$ and within dark matter substructures to crudely reproduce the clump removal procedure applied in Nagai et al. (2007) and Rasia et al. (2006). The cores of the CSF clusters have unphysical cooling flows that must be excised; our choice of core radius affects the position of a cluster on the L–T relation, but not the normalization of the overall L–T relation. Applying this simple analysis procedure to the simulated clusters used in Nagai et al. (2007) gives temperatures that differ by $\sim$10 per cent or less from the mock *Chandra* analysis. The measured X-ray quantities are sensitive to the choice of innermost radius, with larger cuts leading to simultaneously lower measured $L_{\rm bol}$ and $T_{\rm sl}$.

Both of the non-gravitational physics models provide a better match to the observed data than the GO simulation. As discussed in Hartley et al. (2008), the PH haloes match the slope and normalization of the observed L–T relation well. The observed scatter is much larger, however, due primarily to the existence of cool cores in real clusters.

The slope of the CSF haloes also agrees with the observations, but the normalization and scatter are not well matched to the data. The normalization offset is partly due to the lower gas fraction seen in Fig. 1, but the spectral temperatures also play a role. As discussed in Borgani et al. (2004) and Nagai et al. (2007), the temperature profile of the hot phase is steeper than observed in cluster cores, resulting in enhanced $T_{\rm sl}$ values.

In summary, we have shown that both the PH and CSF simulations offer a reasonable match to the form of the L–T relation, but the overall baryon content of haloes differs substantially between the two. In the CSF simulation, star formation is overly efficient, so that nearly 50 per cent of the baryons are in stars rather than in the hot phase. In the PH simulation, the stellar fraction is entirely neglected, but the net heating effect of early galaxy formation is assumed to be large enough to drive the halo baryon fraction substantially below the global value. Neither of these treatments is fully consistent with observations, but they represent two extreme approximations for

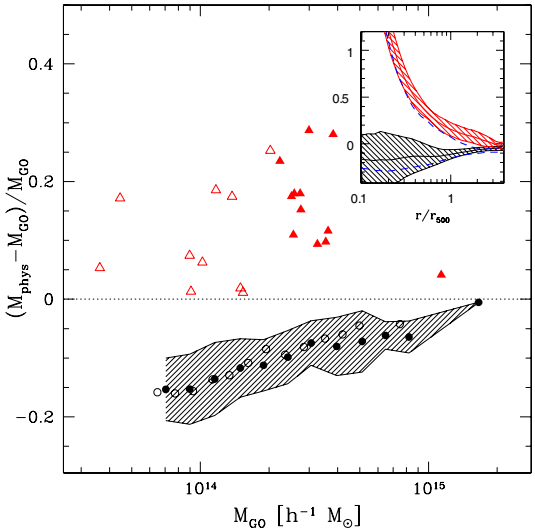

Figure 3. Fractional mass difference in halo mass with respect to the GO realization. Circles show the mean shift for the PH haloes at $z = 0$ (filled) and $z = 1$ (open). Triangles show individual CSF haloes at $z = 0$ (filled) and $z = 1$ (open). The inset panel plots the cumulative radial mass difference for CSF haloes (red) and PH haloes (black) at $z = 0$ (solid, with 1σ scatter) and $z = 1$ (dashed).

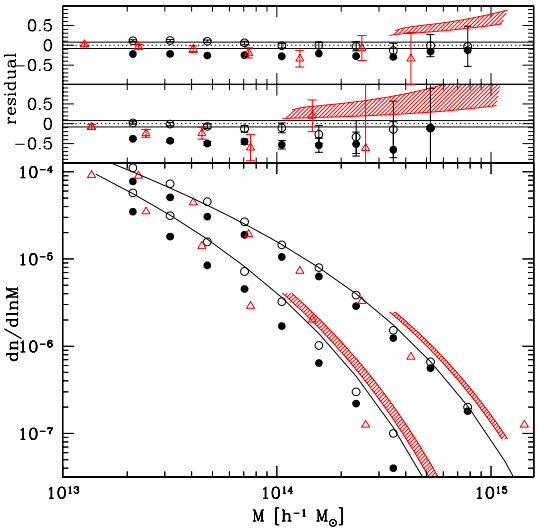

Figure 4. The lower panel shows the halo mass functions for the PH (solid circles) and GO (open circles) versions of the MGS and the ART–GO model (open triangles) at redshifts $z = 0$ (upper) and $z = 1$ (lower). The solid black lines are the TMF expectations at these redshifts. Red bands shows the 90 per cent confidence regions anticipated by the shifts in halo mass for the ART–CSF treatment. The panels above show the fractional difference in number counts between the measured mass functions and the TMF, at $z = 0$ (top) and $z = 1$ (middle). We plot 90 per cent jackknife errors for the ART–GO model, and Poisson errors for the MGS. Note that we have used the TMF for scaling the ART mass functions to match the MGS cosmology.

true behaviour. We next examine the effects that these treatments have on halo mass.

3 HALO MASSES AND THE MASS FUNCTION

Since both pairs of simulations are evolved from the same initial conditions, we are able to match haloes between the realizations performed under the two physical treatments. In Fig. 3, we show the fractional shift in mass that occurs under the PH and CSF treatments, relative to the respective GO model, as a function of GO halo mass at redshifts $z = 0$ and 1. The mean mass shift is plotted for MGS haloes in mass bins. Individual clusters are plotted for the ART simulations at $z = 0$ and 1.

The PH haloes experience a substantial decrease in mass relative to the GO treatments. The magnitude of the $z = 0$ fractional mass shift depends on halo mass, declining from 15 per cent at $10^{14}\,h^{-1}\,M_\odot$ to 5 per cent at $10^{15}\,h^{-1}\,M_\odot$. Although these mass shifts are mostly due to the change in gas fraction, there is also a difference in dark matter structure that enhances the shift. All but the most massive ART–CSF halo show increased mass relative to the respective GO haloes. At the mean mass of the sample at $z = 0$, $3 \times 10^{14}\,h^{-1}\,M_\odot$, the mean fractional mass shift is 0.162 ± 0.022. Approximately, 2 per cent of this shift is due to the increase in baryon mass. The remainder is due to the change in halo structure brought about by baryon cooling (Gnedin et al. 2004; Nagai 2006).

These mass shifts depend on the choice of scale, as shown in the inset of Fig. 3. For comparison with the ART–CSF haloes, we plot the mean mass profile for MGS haloes in the range $1\text{–}3 \times 10^{14}\,h^{-1}\,M_\odot$. Within the core, the mass difference between matched haloes in the MGS simulations is nearly 20 per cent, but the mass difference approaches zero on scales significantly larger than r_{200}. In the ART simulations, we also see that the mass shift is a strong function of scale, within the core it is very high, ∼80 per cent and approaches zero beyond r_{200}. Because of this scale dependence, the magnitude of the mean mass shift and its evolution with redshift is sensitive to our choice of $\Delta = 500\,\rho_c(z)$.

The shifts in mass seen with complex physical treatments will lead to changes in the mass function relative to the GO models. For both MGS simulations and the ART–GO run, we compute binned space densities directly from the simulation counts. Fig. 4 plots these mass functions at redshifts $z = 0$ and 1, and compares them to the TMF expectations for mean density contrasts equivalent to $\Delta_c = 500$, shown by the solid lines. To account for differences in cosmology (primarily the difference in σ_8), we calculate the TMF for both cosmologies. From a fixed number density, we find the mass shift between the two cosmologies, and apply it to the ART–GO data for simple comparison with the MGS mass functions.

The redshift zero GO mass functions match the TMF prediction quite well. The top panels show the fractional difference in counts between the simulations and the TMF, with the 90 per cent statistical calibration uncertainty of the latter shown by the solid, horizontal lines. We include 90 per cent uncertainties on the data points: jackknife uncertainties as a measure of cosmic variance for the ART–GO sample, and Poisson uncertainties for the larger volume of the MGS simulation. The counts of both the ART and MGS models under GO treatment lie within the TMF expectations at $z = 0$.

At all masses, the PH halo mass function is suppressed with respect to the GO halo mass function, at a statistically significant level. At $M_{500} \sim 10^{14}\,h^{-1}\,M_\odot$, the number density of PH haloes is 20 per cent lower than the TMF prediction, a 4σ shift relative to the 5 per cent TMF calibration error. At the very high mass end, $\sim 10^{15}\,M_\odot$, there is consistency with the TMF expectations.

We do not have a complete mass function from the CSF simulation. However, we can anticipate the shift in halo number based on the mean shifts in halo mass presented above. Since the ART–GO models are consistent with the TMF, we derive CSF expectations by shifting the mass by fractional values given by the 90 per cent confidence range of the mean shifts shown in Fig 3,

meaning $\Delta M/M = 0.117 \pm 0.056$ at $z = 1$ and 0.162 ± 0.035 at $z = 0$. We apply these shifts at mass scales probed by the CSF haloes, $M_{500} > 2 \times 10^{14}\, h^{-1}\, \mathrm{M}_{\odot}$. At $z = 0$, the positive shift in halo mass implies upward deviations in number density from the TMF expectation, at levels ranging from 10 to 60 per cent.

4 DISCUSSION AND CONCLUSION

Calibrations of the halo space density from ensembles of *N*-body and dissipationless gas dynamic simulations now have very small statistical uncertainties, ∼5 per cent in number (Tinker et al. 2008). At the high-mass end, this level of precision in number is equivalent to a precision in halo mass at the 2 per cent level. Since baryons represent 17 per cent of the matter density, complex gas dynamics associated with galaxy formation physics could plausibly lead to effects on halo masses of more than a few percent. In this letter, we demonstrate that shifts approaching 10 per cent in mass are possible, and that the sign of this effect is not yet understood.

We use two extreme treatments of gas physics that are likely to bracket the range of behaviour due to astrophysical processes in galaxy clusters. A simple assumption of PH reduces the local baryon fraction in haloes, thereby suppressing their mass at levels ranging from 15 per cent at $10^{14}\, h^{-1}\, \mathrm{M}_{\odot}$ to 5 per cent at $10^{15}\, h^{-1}\, \mathrm{M}_{\odot}$. A more complete physics treatment with cooling and star formation increases the local baryon fraction and deepens the halo potential, thus enhancing halo mass, by an average of 12 per cent at $10^{14.5}\, h^{-1}\, \mathrm{M}_{\odot}$. The effects of cooling and star formation on halo mass are qualitatively consistent with the systematic enhancement in small-scale power seen in previous simulations (Jing et al. 2006; Rudd et al. 2008). In both of the complex physical treatments we consider, the shifts in mass lead to statistically significant offsets in cluster counts from the TMF expectations. These shifts in mass depend on the choice of scale used in defining haloes: in both treatments, the mass shifts are larger when identifying haloes via higher density contrasts.

Although both the PH and CSF simulations provide fair matches to the mean observed *L–T* relation, implying the structure of the hot gas phase is nearly correct, neither describes well the stellar content of clusters. The PH simulation ignores galaxies while the CSF simulation converts nearly ∼50 per cent of baryons into a large stellar component. This is significantly larger than the ∼14 per cent observed by Lin, Mohr & Stanford (2003), and the ∼15–20 per cent observed by Gonzalez, Zaritsky & Zabludoff (2007) when including intracluster light. However, the observational uncertainties on these measurements are still quite large. Although it is tempting to dismiss the PH model due to its lack of detailed physics, a growing body of observations, particularly the ubiquity of strong winds in moderate redshift DEEP2 galaxies (Weiner et al. 2008) and the remarkably simple evolution to $z = 1.4$ of the colour of red sequence galaxies seen in the *Spiter*/Infrared Array Camera on the Spitzer Space Telescope (IRAC) Shallow Survey (Eisenhardt et al. 2008), provide supporting evidence for a scenario in which the fireworks associated with galaxy formation in clusters is both rapid and effective.

Improvements in the physical and computational modelling of cooling and star formation are needed to match the full set of observational constraints on the baryonic mass components of cluster haloes. We have shown here that varying these treatments can affect total halo masses at levels up to 10 per cent. Improving the accuracy of the halo mass function calibration will therefore entail a suite of sophisticated gas dynamic simulations, not more or larger *N*-body simulations.

ACKNOWLEDGMENTS

We thank Elena Rasia, Daisuke Nagai and Jeremy Tinker for their helpful comments. This work was supported in part by NSF AST-0708150. DHR gratefully acknowledges the support of the Institute for Advanced Study. The ART simulations were performed on the Marenostrum supercomputer at the Barcelona Supercomputing Center (BSC). The MGS simulations were performed at Nottingham University, and we thank Frazer Pearce for providing the simulation data.

REFERENCES

Bartelmann M., Steinmetz M., 1996, MNRAS, 283, 431
Bialek J. J., Evrard A. E., Mohr J. J., 2001, ApJ, 555, 597
Bond J. R., Cole S., Efstathiou G., Kaiser N., 1991, ApJ, 379, 440
Borgani S., Governato F., Wadsley J., Menci N., Tozzi P., Lake G., Quinn T., Stadel J., 2001, ApJ, 559, L71
Borgani S. et al., 2004, MNRAS, 348, 1078
Crain R. A., Eke V. R., Frenk C. S., Jenkins A., McCarthy I. G., Navarro J. F., Pearce F. R., 2007, MNRAS, 377, 41
Eisenhardt P. R. M. et al., 2008, ApJ, 684, 905
Ettori S., Dolag K., Borgani S., Murante G., 2006, MNRAS, 365, 1021
Evrard A. E., Henry J. P., 1991, ApJ, 383, 95
Gnedin O. Y., Kravtsov A. V., Klypin A. A., Nagai D., 2004, ApJ, 616, 16
Gonzalez A. H., Zaritsky D., Zabludoff A. I., 2007, ApJ, 666, 147
Gottlöber S., Yepes G., 2007, ApJ, 664, 117
Hartley W. G., Gazzola L., Pearce F. R., Kay S. T., Thomas P. A., 2008, MNRAS, 386, 2015
Holder G., Haiman Z., Mohr J. J., 2001, ApJ, 560, L111
Jenkins A., Frenk C. S., White S. D. M., Colberg J. M., Cole S., Evrard A. E., Couchman H. M. P., Yoshida N., 2001, MNRAS, 321, 372
Jing Y. P., Zhang P., Lin W. P., Gao L., Springel V., 2006, ApJ, 640, L119
Kaiser N., 1991, ApJ, 383, 104
Kravtsov A. V., Nagai D., Vikhlinin A. A., 2005, ApJ, 625, 588
Levine E. S., Schulz A. E., White M., 2002, ApJ, 577, 569
Lima M., Hu W., 2004, Phys. Rev. D, 70, 043504
Lima M., Hu W., 2005, Phys. Rev. D, 72, 043006
Lin Y.-T., Mohr J. J., Stanford S. A., 2003, ApJ, 591, 749
Majumdar S., Mohr J. J., 2003, ApJ, 585, 603
Mazzotta P., Rasia E., Moscardini L., Tormen G., 2004, MNRAS, 354, 10
Nagai D., 2006, ApJ, 650, 538
Nagai D., Vikhlinin A., Kravtsov A. V., 2007, ApJ, 655, 98
Press W. H., Schechter P., 1974, ApJ, 187, 425
Rasia E. et al., 2006, MNRAS, 369, 2013
Reiprich T. H., Böhringer H., 2002, ApJ, 567, 716
Rudd D. H., 2007, PhD thesis, Univ. Chicago
Rudd D. H., Zentner A. R., Kravtsov A. V., 2008, ApJ, 672, 19
Sahlén M. et al., 2008, preprint (arXiv:astro-ph/0802.4462)
Sheth R. K., Tormen G., 1999, MNRAS, 308, 119
Springel V., 2005, MNRAS, 364, 1105
Springel V. et al., 2005, Nat, 435, 629
Stanek R., Evrard A. E., Böhringer H., Schuecker P., Nord B., 2006, ApJ, 648, 956
Sutherland R. S., Dopita M. A., 1993, ApJS, 88, 253
Tinker J. L., Kravtsov A. V., Klypin A., Abazajian K., Warren M. S., Yepes G., Gottlober S., Holz D. E., 2008, ApJ, 688, 709
Vikhlinin A., 2006, ApJ, 640, 710
Voit G. M., Balogh M. L., Bower R. G., Lacey C. G., Bryan G. L., 2003, ApJ, 593, 272
Warren M. S., Abazajian K., Holz D. E., Teodoro L., 2006, ApJ, 646, 881
Weiner B. J. et al., 2008, preprint (arXiv:astro-ph/0804.4686)
White S. D. M., Rees M. J., 1978, MNRAS, 183, 341
Yepes G., Sevilla R., Gottlöber S., Silk J., 2007, ApJ, 666, L61
Younger J. D., Haiman Z., Bryan G. L., Wang S., 2006, ApJ, 653, 27

This paper has been typeset from a TEX/LATEX file prepared by the author.